AD_____

Award Number: DAMD17-99-1-9456

TITLE: Structure of the Tetrameric p53 Tumor Suppressor Bound to DNA

PRINCIPAL INVESTIGATOR: Ronen Marmorstein, Ph.D.

CONTRACTING ORGANIZATION: The Wistar Institute
Philadelphia, PA 19104

REPORT DATE: May 2002

TYPE OF REPORT: FINAL

PREPARED FOR: U.S. Army Medical Research and Materiel Command
Fort Detrick, Maryland 21702-5012

DISTRIBUTION STATEMENT: Approved for Public Release;
Distribution Unlimited

REPORT DOCUMENTATION PAGE

Form Approved
OMB No. 074-0188

1. AGENCY USE ONLY (Leave blank)	2. REPORT DATE	3. REPORT TYPE AND DATES COVERED
	May 2002	Final (15 Apr 99 - 14 Apr 02)

4. TITLE AND SUBTITLE
Structure of the Tetrameric p53 Tumor Suppressor Bound to DNA

5. FUNDING NUMBERS
DAMD17-99-1-9456

6. AUTHOR(S)
Ronen Marmorstein, Ph.D.

7. PERFORMING ORGANIZATION NAME(S) AND ADDRESS(ES)
The Wistar Institute
Philadelphia, PA 19104

E-Mail:Marmor@wistar.upenn.edu

8. PERFORMING ORGANIZATION REPORT NUMBER

9. SPONSORING / MONITORING AGENCY NAME(S) AND ADDRESS(ES)
U.S. Army Medical Research and Materiel Command
Fort Detrick, Maryland 21702-5012

10. SPONSORING / MONITORING AGENCY REPORT NUMBER

11. SUPPLEMENTARY NOTES
Report contains color.

12a. DISTRIBUTION / AVAILABILITY STATEMENT
Approved for public release; distribution unlimited

12b. DISTRIBUTION CODE

13. ABSTRACT ***(Maximum 200 Words)***

The p53 tumor suppressor binds DNA as a tetramer to regulate the transcription of genes involved in cell cycle arrest and apoptosis, and alterations in the DNA-binding core domain of p53 are the most common genetic changes found in breast cancer. The goal of this proposal was to determine the X-ray crystal structure of a p53 tetramer bound to DNA. Towards this goal, we successfully prepared several p53 and short duplex DNA reagents, but have been unable to prepare suitable p53/DNA cocrystals for structure determination. Nonetheless, we have successfully determined the medium resolution (2.7Å) structure of the nascent p53 core domain which we reported in the *Journal of Biological Chemistry*, and have more recently obtained crystal of the p53 core domain that will yield a structure to 2.2Å resolution. Future efforts to obtain a structure of the p53 tetramer bound to DNA will involve cocrystallization with longer DNA targets or DNA targets assembled into nucleosome core particles. The structure of tetrameric p53 bound to DNA will provide new insights into the structural basis underlying p53 mutations, and will provide a framework for the structure-based design of drugs that will be useful in the treatment of p53-mediated breast cancer.

14. SUBJECT TERMS	15. NUMBER OF PAGES
breast cancer	16
	16. PRICE CODE

17. SECURITY CLASSIFICATION OF REPORT	18. SECURITY CLASSIFICATION OF THIS PAGE	19. SECURITY CLASSIFICATION OF ABSTRACT	20. LIMITATION OF ABSTRACT
Unclassified	Unclassified	Unclassified	Unlimited

Table of Contents

(4) INTRODUCTION

The p53 tumor suppressor regulates the transcription of a number of genes involved in cell-cycle arrest and induction of apoptosis in response to cellular or genotoxic stress such as DNA damage or hypoxia (Bargonetti and Manfredi, 2002). The majority of human cancers, including breast cancer, contain p53 alterations, suggesting that the gene plays a central role in the development of cancer and in particular breast cancer [(Hainaut and Hollstein, 2000) and http://www.iarc.fr/p53homepage.html]. The transcriptional activity of p53 is mediated by a tetrameric form of the protein that binds DNA in a sequence-specific fashion to activate or repress the transcription of target genes (El-Deiry et al., 1993; Friedman et al., 1993; Halazonetis and Kandil, 1993; Stenger et al., 1994). p53 contains four functionally distinct domains: a loosely folded N-terminal transcriptional activation domain (residues 1 to 44), a central core (residues 102 to 292) containing a DNA binding domain, a tetramerization region (residues 320 to 356), and a regulatory domain (residues 356-393) (Cho et al., 1994; Pavletich et al., 1993; Wang et al., 1993). The vast majority of tumor-derived p53 mutations are localized to the p53 core (Cho et al., 1994). The overall goal of this proposal was to determine the X-ray crystal structure of a tetrameric form of p53 bound to DNA. The structure would provide a mechanistic basis for how tumor-derived p53 mutants disrupt p53 function and would provide a scaffold for the structure-based design of small molecule compounds that may be useful for reactivation of tumor-derived p53 mutants for the treatment of p53-mediated breast cancer.

(5) BODY

The specific technical objectives of this proposal were to (1) Prepare p53 protein and DNA target sites for p53/DNA cocrystallization (tasks 1-4), (2) Crystallize the p53/DNA complex for structure determination using X-ray crystallography (tasks 5 and 6), (3) Determine the three-dimensional structure of a p53/DNA complex (tasks 7-13), and (4) Overexpress and purify to homogeneity the p53-T284R mutant protein that is able to rescue common tumor-derived p53-mutations, crystallize it bound to DNA, and determine the structure of the p53-T284R/DNA complex (tasks 14-20). For the three year funding period we successfully accomplished tasks 1-6, however technical problems in preparing well diffracting crystals of a true p53 tetramer bound to DNA prevented us from progressing beyond task 6. Nonetheless, our studies have provided important information that may allow us to progress beyond task 6 in the near future and our studies have resulted in reportable outcomes that have already been published or will be published in the near future. A more detailed accounting of our studies is reported below.

With regard to the specific tasks that we had set out to accomplish, we have completed the following: (1) we have cloned in bacteria, overexpressed and purified to homogeneity three protein constructs of mouse p53 that are competent for tetramer formation on DNA; p53(98-292) harboring the p53 core domain, p53(86-351) harboring the core-linker-tetramirization region of p53, and p53(86-391) harboring the core-linker-tetramirization region and regulatory region of p53 (technical objective 1, task 1). In addition, we have cloned and overexpressed, but have not yet purified to homogeneity, a soluble full length mouse p53 protein construct (residues 3-391). (2) We have synthesized and purified to homogeneity several p53 DNA target sites for cocrystallization with our various p53 protein constructs (technical objective 1, task 2). In total we prepared 15 different DNA duplexes ranging in size from 10 to 24 base-pairs. (3) We have characterized the biophysical and DNA-binding properties of each of the purified protein constructs demonstrating that they are monodisperse and capable of binding DNA in a sequence specific fashion (technical objective 1, tasks 3-4). (4) We have carried out extensive p53/DNA cocrystallization efforts employing our various p53 protein constructs and DNA duplex substrates (technical objective 1, tasks 5-6).

In the year one report, we had prepared crystals of an apparent p53(98-292)/DNA complex that diffracted X-rays to a resolution of 2.7Å. In the year 2 report, we reported on completion of the structure determination of the apparent p53(98-292)/DNA complex. Surprisingly, we found that the crystals contained protein, but not DNA. Thus the structure yielded the first image of the p53 core domain in the absence of DNA. The results of this work are described in a publication in the *Journal of Biological Chemistry* and is included in the appendix of this report. During the third year of funding, we successfully obtained a new crystal form of the p53(98-292) construct in the absence of DNA. These crystals diffract to at least 2.2Å resolution and will provide the first high resolution structure of the p53 core domain (Fig. 1 and Table 1). We have recently determined the structure of this new p53 crystal form using the previous structure (at 2.7Å resolution) as a search model, and refinement is underway. Once we complete the refinement of this high resolution p53 core domain structure we will prepare the work for publication.

Based on our results with the p53(98-292) core domain, we conclude that we are unable to obtain crystals of it bound to DNA. Presumably the isolated core domain of p53 does not bind DNA with sufficient specificity to facilitate cocrystallization with DNA. Therefore, most of our efforts during the third year of the funding period has gone towards cocrystallization efforts of longer p53 constructs with DNA. For these efforts, we have relied on cocrystallization with the p53(86-351) and p53(86-391) constructs that we had already prepared. Unfortunately, we have yet been able to cocrystallize these protein constructs with DNA. Simply mixing our p53 protein constructs with DNA have resulted in the formation of heavy precipitate that have thwarted our cocrytallization efforts. The addition of low concentrations (about 20 mM) of divalent metal ion or high concentrations of monovalent metal ion (500 mM) has served to prevent such precipitation, but have not produced cocrystals. We have evidence that the reason for this is that the added metal ions dissociate the protein/DNA complex. We had obtained one crystal form that was formed in the presence of p53(86-351) that diffracted to high resolution, but after collecting diffraction data and solving the structure we determined that the crystals contained only the tetramirization domain of p53 (which presumably had formed through proteolysis of the full length protein construct). Since the crystal structure of the p53 tetramirization domain had previously been reported (Jeffrey et al., 1995), we abandoned any further work on this protein construct. We conclude that the successful cocrystallization of tetrameric forms of p53 bound to DNA will require dramatically different DNA target sites and or other protein cofactors. This will be further discussed in the CONCLUSIONS section.

(6) KEY RESEARCH ACCOMPLISHMENTS

- Medium resolution structure determination and publication of the mouse p53 core domain [p53(98-292)].
- High resolution structure determination of the mouse p53 core domain.
- Overexpression and purification to homogeneity of several mouse p53 protein constructs harboring the core domain (CD), linker region (L), and tetramerization domain (TD); harboring the CD-L-TD and DNA regulatory region (DR).
- Overexpression and partial purification of a full-length mouse p53 protein construct [p53(3-391)].

(7) REPORTABLE OUTCOMES

Zhao, K., Chai, X., Johnston, K., Clements, A. and Marmorstein, R. "Crystal structure of the mouse p53 core DNA-binding domain at 2.7Å resolution," (2001) *J. Biol. Chem.*, 276, 12120-12127.

(8) CONCLUSIONS

During the three year funding period of this proposal we successfully prepared three mouse p53 protein constructs for cocrystallization efforts, one harboring the isolated core domain [p53(98-292)], another harboring the core domain, linker and tetramerization domain [p53(86-351)], and another harboring the core domain, linker, tetramerization domain and regulatory region [p53(86-391)]. We have also successfully prepared various DNA duplexes (ranging in size from 10-24 base-pair) for cocrystallization efforts and several cocrystallization efforts have been attempted without success. Taken together, we have successfully completed tasks 1-5 of this proposal but have been stalled at task 6 due to our inability of cocrystallize a true p53 tetramer bound to DNA. Although we were unable to cocrystallize these protein constructs with DNA, we successfully completed the medium resolution structure determination of the nascent core domain which was published in the *Journal of Biological Chemistry*, and a high resolution refinement of the core domain crystallized in a different form is being refined for future publication.

Based on our results to date, we conclude that successful cocrystallization of tetrameric forms of p53 bound to DNA will require dramatically different DNA target sites and or other protein cofactors. We are encouraged by a recent report by Dr. Emerson's laboratory showing that the p53 protein binds DNA in chromatin or long DNA targets much more avidly than short oligonucleotides (Espinosa and Emerson, 2001). In addition this study show that the C-terminal regulatory region is required for chromatin binding by p53. Other recent reports also show that long DNA fragments promote p53 binding by forming secondary structures .(Jett et al., 2000; Kim et al., 1999). Together, these studies suggest that the p53(86-351) and p53(86-391) protein constructs are suitable constructs for DNA cocrystallization efforts, but that longer DNA fragments of DNA in the context of a nucleosome particle may be more suitable as DNA substrates. In light of these studies, future p53/DNA cocrystallization efforts will employ p53 targets assembled into a nucleosome core particle (Luger et al., 1997) or considerably longer p53 target duplexes harboring one or more tetramer p53 binding sites (Espinosa and Emerson, 2001).

(9) REFERENCES

Bargonetti, J., and Manfredi, J. J. (2002). Multiple roles of the tumor suppressor p53. Curr. Opin. Oncol. *14*, 86-91.

Cho, Y., Gorina, S., Jeffrey, P. D., and Pavletich, N. P. (1994). Crystal structure of a p53 tumor suppressor-DNA complex: understanding tumorigenic mutations. Science *265*, 346-355.

El-Deiry, W. S., Tokino, T., Velculescu, V. E., Levy, D. B., Parsons, R., Trent, J. M., Lin, D., Mercer, W. E., Kinzler, K. W., and Vogelstein, B. (1993). WAF1, a potential mediator of p53 tumor suppression. Cell, 817-825.

Espinosa, J. M., and Emerson, B. M. (2001). Transcriptional regulation by p53 through intrinsic DNA/chromatin binding and site-directed cofactor recruitment. Mol. Cell *8*, 57-69.

Friedman, P. N., Chen, X. B., Bargonetti, J., and Prives, C. (1993). The p53 protein is an unusually shaped tetramer that binds directly to DNA. Proc Natl Acad Sci U S A *90*, 5878-5878.

Hainaut, P., and Hollstein, M. (2000). p53 and human cancer: the first ten thousand mutations. Adv Cancer Res *77*, 81-137.

Halazonetis, T. D., and Kandil, A. N. (1993). Conformational shifts propagate from the oligomerization domain of p53 to Its tetrameric DNA-binding domain and restore DNA-binding to select p53 mutants. EMBO J *12*, 5057-5064.

Jeffrey, P. D., Gorina, S., and Pavletich, N. P. (1995). Crystal structure of the tetramerization domain of the p53 tumor suppressor at 1.7 angstroms. Science *267*, 1498-1502.

Jett, S. D., Cherny, D. I., Subramaniam, V., and Jovin, T. M. (2000). Scanning force microscopy of the complexes of p53 core domain with supercoiled DNA. J. Mol. Biol. *299*, 585-592.

Kim, E., Rohaly, G., Heinrichs, S., Gimnopoulos, D., Meissner, H., and Deppert, W. (1999). Influence of promoter DNA topology on sequence-specific DNA binding and transactivation by tumor suppressor p53. Oncogene *18*, 7310-7318.

Luger, K., Mader, A. W., Richmond, R. K., Sargent, D. F., and Richmond, T. J. (1997). Crystal structure of the nucleosome core particle at 2.8 angstrom resolution. Nature *389*, 251-260.

Pavletich, N. P., Chambers, K. A., and Pabo, C. O. (1993). The DNA binding domain of p53 contains the four conserved regions and the four major mutation hot spots. Genes & Develop *7*, 2556-2564.

Stenger, J. E., Tegtmeyer, P., Mayr, G. A., Reed, M., Wang, Y., Wang, P., Hough, P. V. C., and Mastrangelo, I. A. (1994). p53 oligomerization and DNA looping are linked with transcriptional activation. EMBP J *13*, 6011-6020.

Wang, Y., Reed, M., Wang, P., Stenger, J. E., Mayr, G., Anderson, M. E., Swhwedes, J. F., and Tegtmeyer, P. (1993). p53 domains: identification and characterization of two atonomous DNA-binding domains. Genes & Dev *7*, 2575-2586.

(10) APPENDICES

Figure 1

Table 1

Zhao, K., Chai, X., Johnston, K., Clements, A. and Marmorstein, R. "Crystal structure of the mouse p53 core DNA-binding domain at 2.7Å resolution," (2001) *J. Biol. Chem.*, 276, 12120-12127.

(11) PERSONNEL RECEIVING PAY FROM THIS EFFORT

Ronen Marmorstein
Kehao Zhao
Santosh Hodawadekar
Karen Johnston
Arienne Poux

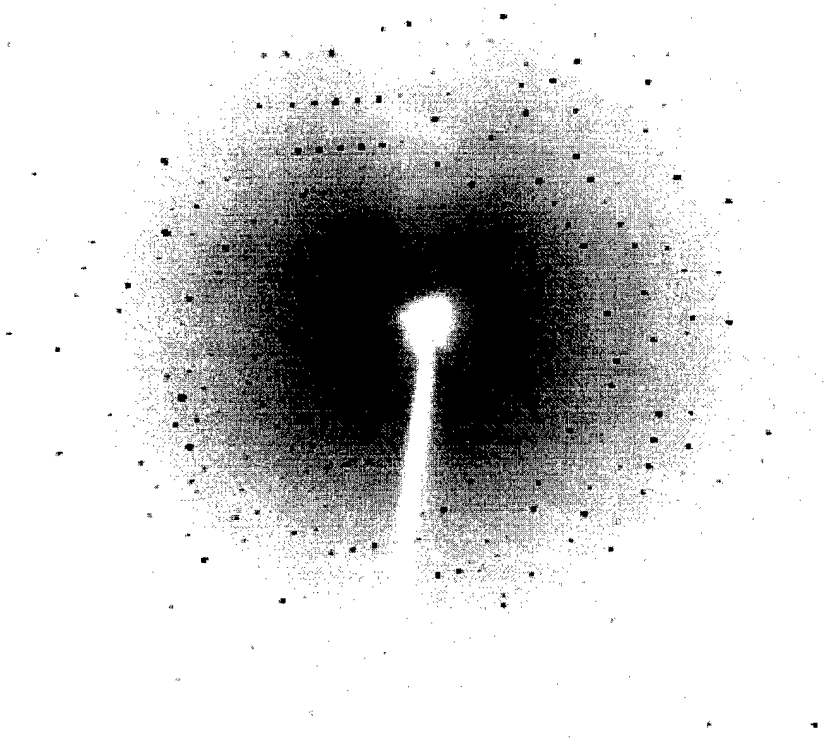

Figure 1. High resolution X-ray diffraction from crystals of the core domain of p53 (residues 98-292). The highest resolution reflection occurs at 2.10 Å.

Table 1. Summary of crystallographic parameters for crystals of p53(98-292).

Parameter	*C*2
Cell parameters	a=92.07Å b=44.51Å c=62.78Å
no. of observations	119272
no. of unique reflections	12252
Monomer per Asy. Unit	1
Vm ($Å^3$)	2.36
resolution (Å)	2.10 Å
overall completeness (last shell)	94 (92.6) %
Overall I/sigma (last shell)	19.36 (5.67) %
*R*merge (last shell)	6.5 (24.2) %

THE JOURNAL OF BIOLOGICAL CHEMISTRY
Vol. 276, No. 15, Issue of April 13, pp. 12120–12127, 2001
Printed in U.S.A.

Crystal Structure of the Mouse p53 Core DNA-binding Domain at 2.7 Å Resolution*

Received for publication, December 22, 2000
Published, JBC Papers in Press, January 4, 2001, DOI 10.1074/jbc.M011644200

Kehao Zhao‡, Xiaomei Chai‡, Karen Johnston‡, Adrienne Clements‡§, and Ronen Marmorstein‡§¶‖

From the ‡The Wistar Institute and the ¶Department of Chemistry, University of Pennsylvania and the §Department of Biochemistry and Biophysics, University of Pennsylvania School of Medicine, Philidelphia, Pennsylvania 19104

The p53 tumor suppressor is a sequence-specific DNA-binding protein that activates transcription in response to DNA damage to promote cell cycle arrest or apoptosis. The p53 protein functions in a tetrameric form *in vivo* and contains four domains including an N-terminal transcriptional activation domain, a C-terminal regulatory domain, a tetramerization domain, and a central core DNA-binding domain that is the site of the majority of tumor-derived mutations. Here we report the 2.7-Å crystal structure of the mouse p53 core domain. Like the human p53 core domain in complex with DNA, the mouse p53 core domain adopts an immunoglobulin-like β sandwich architecture with a series of loops and short helices at opposite ends of the β sandwich. Comparison of the DNA-bound and DNA-free p53 core domains reveals that while the central β sandwich architecture remains largely unchanged, a loop region important for DNA binding undergoes significant rearrangement. Although this loop region mediates major groove DNA contacts in the DNA-bound structure, it adopts a conformation that is incompatible with DNA binding in the DNA-free structure. Interestingly, crystals of the DNA-free core domain contain a noncrystallographic trimer with three nearly identical subunit-subunit (dimer) contacts. These dimer contacts align the p53 core domains in a way that is incompatible with simultaneous DNA binding by both protomers of the dimer. Surprisingly, similar dimer contacts are observed in crystals of the human p53 core domain with DNA in which only one of the three p53 protomers in the asymmetric unit cell is specifically bound to DNA. We propose that the p53 core domain dimer that is seen in the crystals described here represents a physiologically relevant inactive form of p53 that must undergo structural rearrangement for sequence-specific DNA binding.

The p53 tumor suppressor protein functions as a checkpoint during the G_1/S cell cycle transition, responding to DNA damage by activating transcription of genes that encode proteins inducing cell cycle arrest or apoptosis (1, 2). Disruption of the G_1/S cell cycle transition and mutation of the p53 protein in particular occur in a variety of cancer types and correlate with the majority of human cancers (3).[1] The majority of p53 tumor-derived mutations are now known to inactivate its DNA binding properties and therefore to impair its ability to activate transcription (4).

The transcriptional activity of p53 is mediated by a tetrameric form of the protein that binds DNA in a sequence-specific fashion to activate the transcription of target genes (5–8). Each p53 subunit contains four functionally distinct domains: a loosely folded N-terminal transcriptional activation domain (residues 1–44), a central core (residues 102–292) containing a DNA-binding domain, a tetramerization region (residues 320–356), and a regulatory domain (residues 356–393) (4, 9, 10). There are over 100 naturally occurring p53 DNA target sequences, and the human genome has been estimated to contain about 200–300 of such sites (11). Although the sequences of these p53 DNA target sites show variability, they all contain two head to tail decamers each containing a pentameric inverted repeat. Most decamers contain the consensus sequence PuPuPuC(A/t) ↓ (T/a)GPyPyPy, where Pu and Py are purines and pyrimidines, respectively (12). Although the various domains of the p53 protein can function autonomously, *in vivo* activity requires the intact protein. In addition, various lines of evidence suggest that the intact protein exists in two conformational states, one that has low affinity for DNA (T state) and another that has a high affinity for DNA (R state) (6, 13).

Significant insights into the tetramerization and DNA binding properties of p53 are revealed by the structures of the isolated tetramerization domain (14–16) and of the human p53 core domain bound as a monomer to DNA (4), respectively. The structure of the tetramerization domain reveals a dimer of dimers. The structure of the p53 core domain bound to DNA reveals the details of monomer binding to a pentameric DNA sequence. These findings were used to rationalize the functional consequence of the majority of tumor-derived p53 mutations by showing that they map to regions of the core domain that would either affect the stability of the core domain itself or destabilize protein-DNA contacts. Despite the insights that are gained from the structural analysis of p53, several questions underlying p53 structure/function still remain. Among these questions is the issue of the nature of the structural rearrangements that p53 undergoes upon DNA binding.

We report here the crystal structure of the mouse p53 core domain in the absence of DNA. A comparison with the crystal structure of the human p53 core domain bound as a monomer to DNA reveals that the overall structure of the core domain remains largely unperturbed upon DNA binding except for a

* This work was supported by Grant DAMD17-99-1-9456 from the United States Army Breast Cancer Research Program (to R. M.). The costs of publication of this article were defrayed in part by the payment of page charges. This article must therefore be hereby marked "*advertisement*" in accordance with 18 U.S.C. Section 1734 solely to indicate this fact.

The atomic coordinates and structure factors (code 1HU8) have been deposited in the Protein Data Bank, Research Collaboratory for Structural Bioinformatics, Rutgers University, New Brunswick, NJ (http://www.rcsb.org/).

‖ To whom correspondence should be addressed: The Wistar Inst., 3601 Spruce St., Philadelphia, PA 19104. Tel: 215-898-5006; Fax: 215-898-0381; E-mail: marmor@wistar.upenn.edu.

[1] Contact the corresponding author for an additional Web address.

pronounced movement of a loop region. This loop region adopts a conformation that is incompatible with DNA binding in the DNA-free structure but adopts a conformation that facilitates major groove DNA contacts in the DNA-bound structure. Moreover, the crystals analyzed here, reveal a noncrystallographic trimer with three nearly identical subunit-subunit (dimer) contacts. These dimer contacts align the p53 core domains in a way that is incompatible with simultaneous DNA binding by both protomers of the dimer. Interestingly, similar dimer contacts are observed in crystals of the human p53 core domain with DNA in which only one of three p53 protomers in the asymmetric unit cell is specifically bound to DNA. We discuss the implications of these findings for DNA-induced structural rearrangements of the p53 core domain in the context of the intact p53 tetramer.

TABLE I
Data collection and refinement statistics

Space group	$C222_1$
Cell dimensions (Å)	a = 73.68
	b = 119.99
	c = 184.24
Resolution (Å)	10–2.7
No. of observations	121009
No. of unique reflections	22733
Completeness/last shell	99.5/98.7%
Multiplicity	5.3
I/σ(I)/last shell	9.6/3.9
R-merge[a]/last shell	0.051/0.189
No. of reflections ($F > 2\sigma(F)$)	22252
No. of protein atoms	4381
No. of zinc atoms	3
No. of water atoms	108
R-factor[b]	23.9
R-free[c]	29.9
Mean B value (Å)	67.2
r.m.s.d. bonds (Å)[d]	0.007
r.m.s.d. angles (°)	1.32
Dihedral angles (°)	25.0
Improper angles (°)	0.89

[a] R-merge = $\Sigma_h\Sigma_i|I_{h,i} - I_h|/\Sigma_h\Sigma I_{h,i}$ where I_h is the mean intensity of symmetry-related reflections, $I_{h,i}$.
[b] R-factor = $\Sigma||F_o| - |F_c||/\Sigma|F_o|$ where F_o and F_c are the observed and calculated structure factor amplitudes, respectively.
[c] R-free is calculated for the 10% of the data that was withheld from refinement.
[d] r.m.s.d., root mean square deviation.

MATERIALS AND METHODS

Purification and Crystallization of the Mouse p53 Core Domain—The DNA sequence encoding the mouse p53 core domain (residues 92–292) was amplified from the plasmid p11-4 (obtained from A. Levine, Princeton University) by polymerase chain reaction and subcloned into the pRSET (Invitrogen) bacterial expression vector. The plasmid was transformed into the *Escherichia coli* BL21/DE-3 strain. Cells were initially grown in LB medium at 37 °C. When cultures reached an absorbance at 595 nm of ~0.4–0.6, cells were induced by the addition of 0.5 mM isopropyl-1-thio-β-D-galactopyranoside (supplemented with 100 μM zinc acetate) and grown overnight at 15 °C. The cells were isolated by centrifugation and resuspended in low salt buffer A (20 mM sodium citrate, pH 6.1, 100 mM NaCl, 10 μM Zn^{2+}, and 10 mM dithiothreitol). The cells were sonicated, and cellular debris was removed by centrifugation. The supernatant containing soluble mouse p53 core domain was loaded onto a SP-Sepharose (Amersham Pharmacia Biotech) ion exchange column, which was washed with 20× column volumes of buffer A, and the protein was eluted with a 0.1–1.0 M NaCl gradient. Peak fractions containing p53 core domain were pooled and concentrated using a Centriprep-10 (Amicon) and further purified by gel filtration chromatography using a Superdex-75 column. Peak fractions were judged to be greater than 97% homogeneous by SDS-polyacrylamide gel electrophoresis analysis, concentrated to ~40–55 mg/ml, and stored at −80 °C until further use.

Crystallization attempts were initially directed at obtaining a complex of the p53 core domain bound as a tetramer to a 24-base-paired DNA duplex containing four pentameric DNA binding sites. To this end, 10 mg/ml protein was mixed with a 0.25 molar equivalent of DNA duplex and screened for crystallization against a crystallization screen

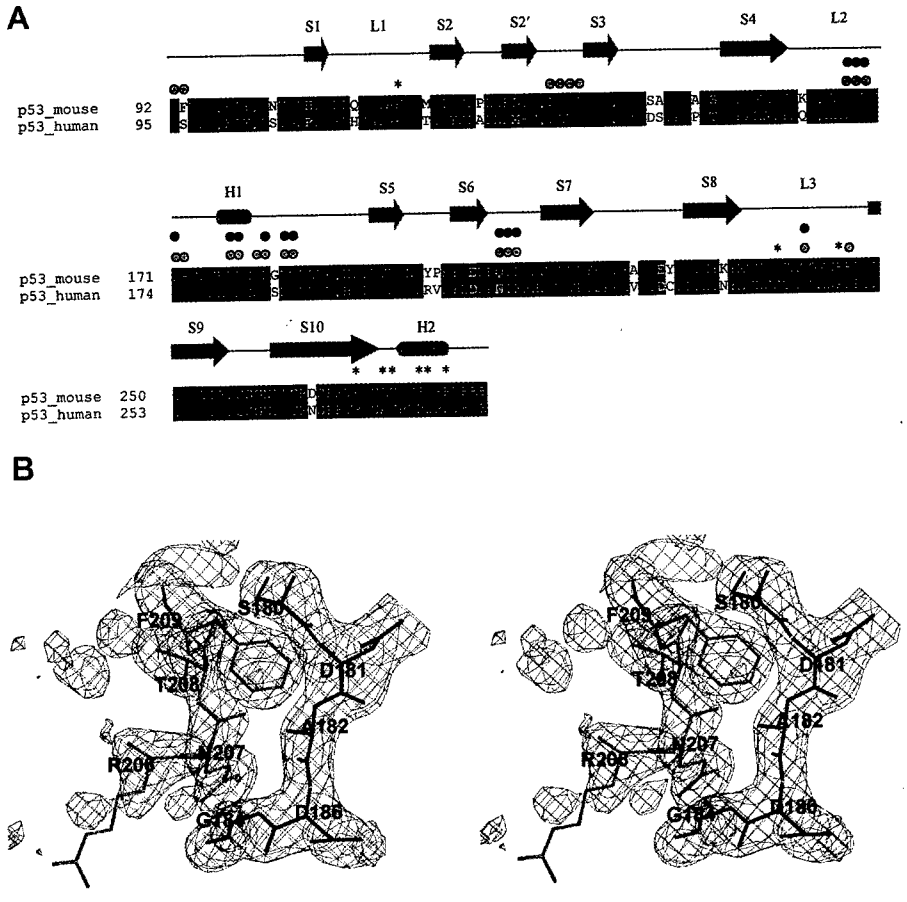

FIG. 1. *A*, sequence alignment of the p53 core domains from mouse and human. Sequences are aligned using the CLUSTAL program and displayed with the BOXSHADE program. *Black* and *gray backgrounds* are used to indicate identical and conserved residues at a given position, respectively. Secondary structural elements within the mouse p53 core domain are shown above the sequence alignment. The *circle* symbols indicate residues that are associated with the dimer interface of the mouse DNA-free (*black circle*) and human DNA-bound (*gray circle*) p53 core domain, and the * symbol indicates residues of the human p53 core domain that contact DNA in the human p53 core-DNA complex. *B*, representative $F_o - F_c$ omit electron density map of the refined mouse p53 core domain structure proximal to the dimer interface. The map is contoured at 2.5 σ. The *green* and *red* colors indicate molecules A and B of the p53 core domain within the asymmetric unit cell.

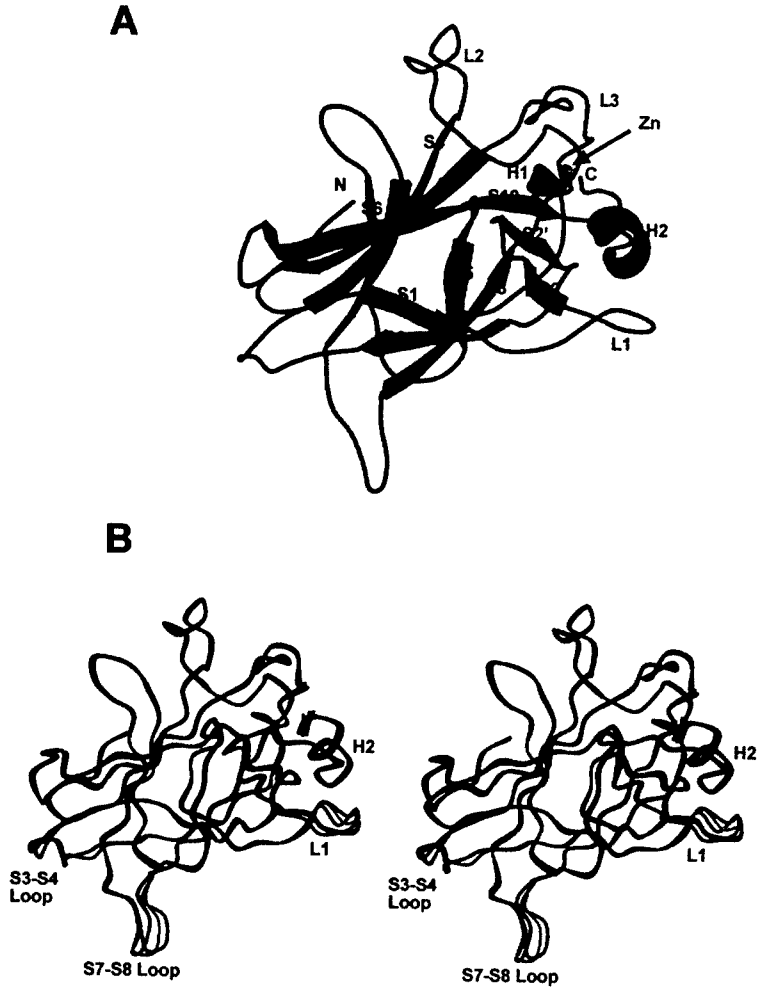

FIG. 2. **Overall structure of the mouse p53 core domain.** *A*, schematic ribbon diagram of the p53 core domain. *B*, Cα superposition of the three p53 protomers in the asymmetric unit cell of the crystals.

for protein-DNA complexes using the hanging drop method. The best crystals were obtained against a reservoir containing 8% polyethylene glycol 4000, 200 mM KCl, 50 mM $MgCl_2$, 10 mM dithiothreitol, and 50 mM Tris-HCl, pH 7.5, and grew to a typical size of 0.2 × 0.4 × 0.4 mm. Subsequent washing of large well formed crystals followed by crystal dissolution and analysis on SDS-polyacrylamide gel electrophoresis and silver staining revealed that these crystals contained the p53 core domain but no DNA.

Data Collection, Structure Determination, and Refinement—Crystals of the mouse p53 core domain were flash-frozen in a cryoprotectant containing the reservoir solution supplemented with 25% polyethylene glycol 400, and diffraction data were collected at 120 K at the A1 station of Cornell High Energy Synchrotron Source using a charged coupled device detector. Data were processed and scaled with MOLSFLM (17). Crystals belong to the orthorhombic space group $C222_1$ with three molecules in the asymmetric unit. The structure was solved by molecular replacement with the program AMoRe (18) using diffraction data from 10 to 3.0 Å. The search model used in the calculation was molecule B of the human p53 core domain (accession number 1TSR). For the search model, residues that differed between the human and mouse p53 core domains were changed to alanine (except for residues 183 and prolines that were changed to glycines). Rotation and translation searches followed by rigid body refinement yielded an unambiguous solution for the three protomers in the asymmetric unit cell with an *R*-factor of 47.5% and a correlation value of 42.4%.

The model was manually rebuilt against $2F_o - F_c$, $F_o - F_c$, and $F_c - F_o$ maps using the program O (19). Rigid body refinement, least square minimization, and simulated annealing refinement with crystallography and NMR suite (20) using noncrystallographic symmetry restraints between the three protomers in the asymmetric unit cell were carried out at a resolution range of 10–3.0 Å. When the data were extended to a 2.7-Å resolution, noncrystallographic symmetry restraints were gradually released, and several cycles of simulated annealing (21), torsion angle dynamic (22), temperature factor refinement, and manual model building were carried out. During the final stages of refinement, a bulk solvent correction was applied to the data (23), water molecules were included using the waterpick routine of crystallography and NMR suite, and three zinc ions were added. Some residues at the very N and C termini were not visible in the electron density map and were therefore not modeled. The final structure contained residues 99–284 of each protomer, had excellent stereochemistry, and had crystallographic *R*-factors of 23.9 and 29.9% for *R*-working and *R*-free, respectively, against data from 10 to 2.7 Å (see Table I and Fig. 1*B*).

Sedimentation Equilibrium Ultracentrifugation—For sedimentation equilibrium experiments, each cell was assembled with a double sector 12-mm centerpiece with sapphire windows. Blank scans with distilled water were taken before interference optics sedimentation equilibrium experiments at appropriate speeds to correct for window distortion of the fringe displacement data (24). Cells were loaded with the mouse p53 core at two different starting concentrations (0.5 and 1.5 mg/ml) in a buffer containing 100 mM NaCl, 10 mM dithiothreitol, and 20 mM Tris-HCl, pH 7.5. The experiment was performed at three separate centrifugation speeds of 22,900, 32,400, and 37,500 rpm. At each speed, fringe displacement scans were collected every 4 h until the protein samples reached equilibrium. Equilibrium was assessed by comparison of successive scans using the MATCH program, and data editing was performed using the REEDIT program (both programs were provided by National Analytical Ultracentrifugation Facility, Storrs, CT).

After equilibrium was obtained, the NONLIN program (25) was used to globally fit the final scans from the two different concentrations and all speeds (a total of six curves were analyzed simultaneously). NONLIN fits used an effective reduced molecular weight, $\sigma = M(1 - \bar{v}\rho)\omega^2/RT$, in which M is the molecular weight, $\bar{v}$ is the partial specific volume, ρ is the solvent density, ω is the angular velocity (2π(rpm)/60), R is the gas constant, and T is the temperature in Kelvin. The partial specific volume of the mouse p53 core was calculated from the amino acid sequence, and the density of the solvent was calculated as described previously (26). For this model of weak self-association, σ was held at the correct value based on the known monomer molecular weight of the protein, and separate equilibrium constants for each scan were fitted as ln K. These values were converted to dissociation constants with the appropriate molar units. The fit quality for the model

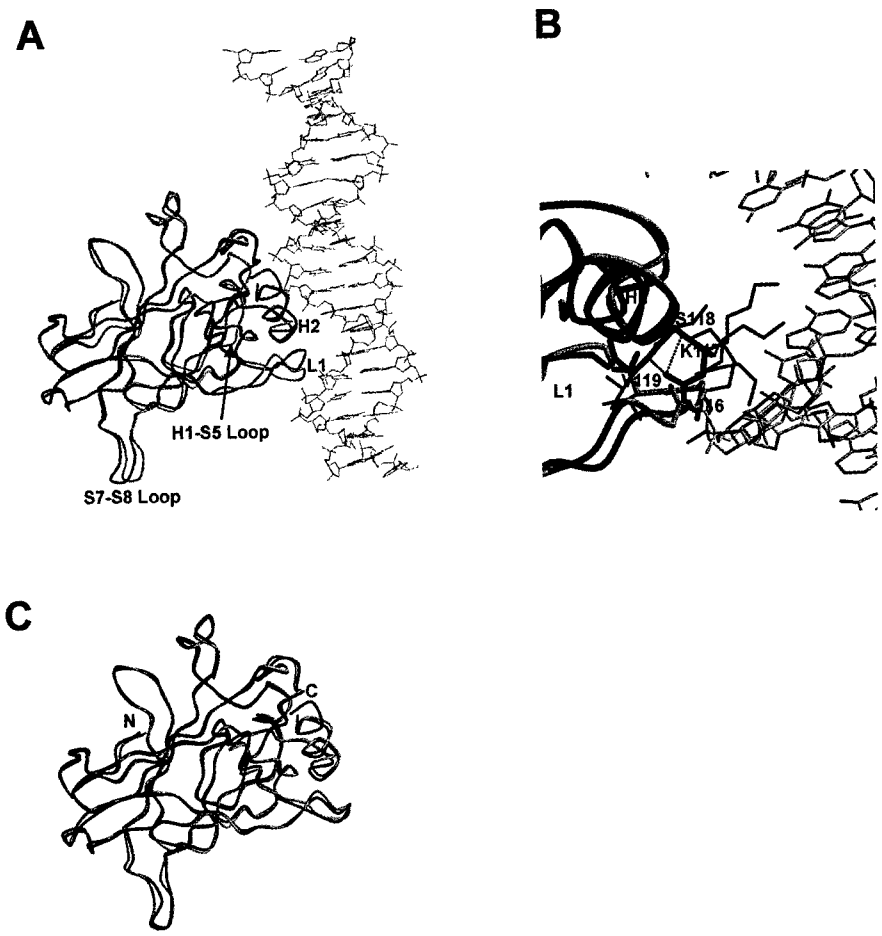

FIG. 3. **Comparison of the DNA-free form of the mouse p53 core domain with the DNA-bound and DNA-free forms of the human p53 core domain.** The DNA-free mouse p53 core domain is shown in *green*, and the human p53 core domain is shown in *red*. *A*, Cα superimposition of the DNA-free mouse p53 core domain with the DNA-bound form of the human p53 core domain. The DNA that is bound to the human p53 core domain is shown in *blue*. *B*, close-up view of the p53-DNA interface proximal to the L1 loop (*A*). The DNA-bound form of the human p53 core domain is shown in *red*, highlighting residues 116–119 of the L1 loop (mouse p53 numbering). The corresponding region of molecule A of the DNA-free mouse p53 core domain is shown in *gray*. The conformations of the Lys-117 side chain in the three mouse p53 core domains in the asymmetric unit cell are shown in *dark gray*. *C*, Cα superimposition of the DNA-free mouse p53 core domain with the DNA-free form of the human p53 core domain.

was determined by examination of residuals and by minimization of the fit variance. The root mean square deviation of the residuals for the multiple species model was 9.56×10^{-3}.

RESULTS AND DISCUSSION

Overall Structure of the p53 Core Domain—The crystal structure presented here contains three molecules of the mouse p53 core domain in the asymmetric unit cell. The overall fold of the p53 core domain is very similar to that of the previously reported core domain in complex with DNA (4) (Figs. 1*A* and 2*A*). Briefly, the core domain forms a central region that adopts an immunoglobulin-like β sandwich architecture of two long twisted antiparallel β sheets of four (S1, S3, S8, and S5) and five (S10, S9, S4, S7, and S6) strands (Figs. 1*A* and 2*A*). Located at opposite ends of the β sandwich are a series of loops. One of the two ends also contains two short helices (H1 and H2) and a tightly bound zinc atom that is tetrahedrally ligated by Cys-173 and His-176 from the L2 loop (between strands S4 and S5) and Cys-235 and Cys-239 from the L3 loop (between strands S8 and S9). The structure of the human p53 core domain bound to DNA shows that the H2 helix, the L3 loop, and the L1 loop (between strands S1 and S2) interact with DNA.

A superposition of the three molecules in the asymmetric unit (Fig. 2*B*) gives root mean square deviation values of 0.40 Å (molecule A-molecule B), 0.57 Å (molecule C-molecule A), and 0.62 Å (molecule B-molecule C) for all main chain atoms. Structural deviations are largely restricted to the L1 loop (residues 115–121) along the DNA-binding side of the core domain and the loops between strands S3 and S4 (residues 220–223) and S7 and S8 (residues 149–151) opposite to the DNA-binding side of the molecule. Although the structural variability within the S3-S4 and S7-S8 loops appears to reflect inherent flexibility within this region of the core domain, as will be discussed below, the structural variability within the L1 loop appears to be due in part to the absence of bound DNA.

Comparison with the Human p53 Core Domain in Complex with DNA—The core domains of human and mouse p53 are highly homologous in sequence with an overall identity of 89%. Therefore a comparison between the nascent mouse p53 core domain and the DNA-bound human p53 core domain can be used to examine the effect of core domain structure as a function of DNA binding. An overall comparison of the nascent (using monomer A) and the DNA-bound form of p53 shows a root mean square deviation between main chain atoms of 0.87 Å as compared with a value between 0.4 and 0.62 Å between noncrystallographically related subunits of the nascent structure (Fig. 3*A*). The larger structural differences that are observed when comparing the unbound and DNA-bound forms of p53 within two different crystal forms are consistent with a comparison between the p53 core domain in the absence of DNA with the DNA-free p53 subunit within the crystal lattice of the p53-DNA complex (Fig. 3*C*). This comparison shows a root mean square deviation between main chain atoms of 0.57 Å. Taken together, DNA binding by the p53 core domain appears to illicit small yet significant structural changes.

The structural changes between the DNA-bound and DNA-free core domains are primarily localized to four regions (Fig. 3*A*). Near the DNA-binding surface structural differences are seen in the L1 loop and the C-terminal end of the H2 helix. Away from the DNA-binding surface structural differences are seen in the loop separating the S7 and S8 strands and the loop between the H1 helix and the S5 strand. Structural differences within the S7-S8 and H1-S5 loops appear to be a function of interactions between the p53 core domains in the crystals, as will be discussed below, whereas structural differences within

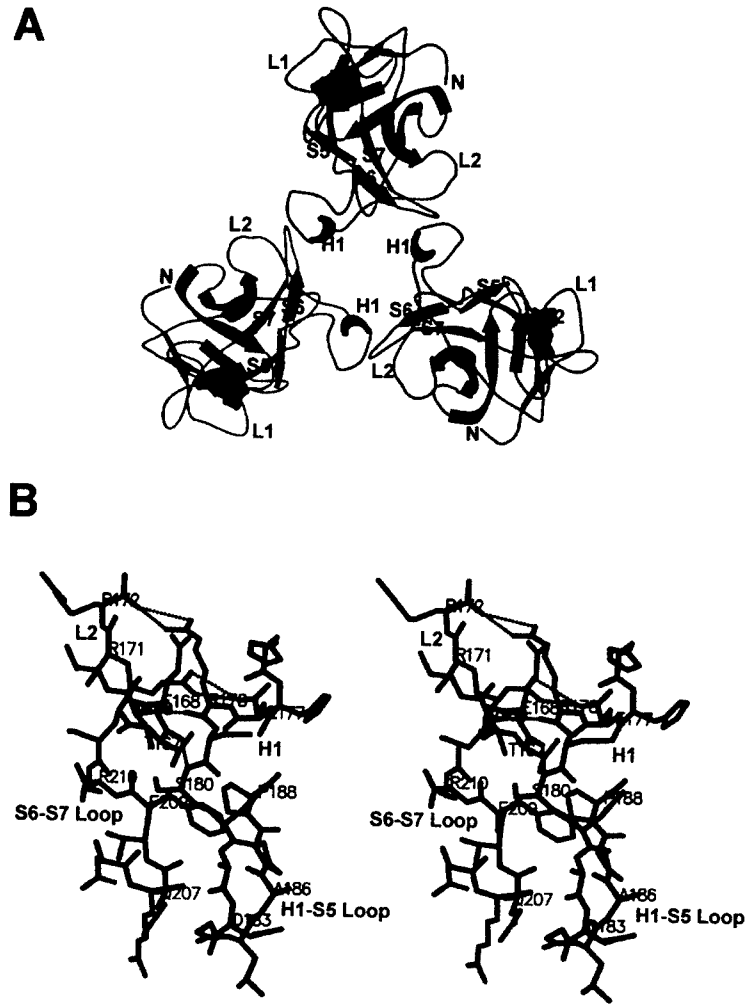

FIG. 4. **Structure of the mouse p53 core domain dimer.** *A*, trimeric packing of the mouse p53 core domain in the asymmetric unit cell viewed perpendicular to the 3-fold axis of the trimer. *B*, stereo diagram showing the intermolecular interaction at the dimer interface of the trimeric structure. Protomer A is shown in *green*, and protomer B is shown in *blue*. *C*, superposition of the mouse p53 core domain dimer (using protomers A and B) with the p53 core domain dimer in crystals of the human core domain in which only one of the two protomers is specifically bound to DNA. The *left view* shows an overall superposition of the dimers, and the *right view* shows a superposition of only one of the protomers of the dimer. This type of superposition shows that the second protomers of the respective dimers are related by a 12 ° rotation. *D*, dimer contacts within the crystals of the human p53 core domain in which only one of the two protomers is specifically bound to DNA.

the L1 loop appear to be a function of DNA binding.

The L1 loop in the DNA-free form of the p53 core is further away from the H2 helix than it is in the DNA-bound form. In fact, a superposition of the DNA-free p53 core onto the core domain of the DNA complex suggests that the L1 loop would clash with the DNA and therefore suggests that the L1 loop would need to move closer to the H2 helix (as it is in the DNA-bound structure) to fit into the major groove of the DNA. Two interactions within the L1 loop appear to stabilize its DNA-bound form over the DNA-free form. Within the L1 loop, Lys-117 (Lys-120 in human p53) is disordered in all three core domains of the asymmetric unit cell (Fig. 3*B*). In contrast, the DNA complex shows that Lys-120 makes contacts to the major groove of the DNA. The conformation of the L1 loop in the DNA bound form is also stabilized by a backbone H bond at the turn of the L1 loop between Ala-116 and Ser-118 (mouse p53 numbering), an interaction that is lost in the DNA-free form (Fig. 3*B*). Taken together, the L1 loop region of the p53 core appears to undergo important structural rearrangement for DNA binding.

Dimer Contacts between p53 Core Domains in the Crystals—The most surprising finding from our crystal structure is that the mouse p53 core domain is packed in the crystals as a noncrystallographic trimer in which the subunits are held together by nearly identical dimer contacts. These dimer contacts are quite extensive and bury a total of ~1458 Å^2 at each interface, which amounts to ~15% of the surface area of each protein subunit (Fig. 4*A*). These dimer contacts involve the H1-S5 loop of one subunit and the S4-H1 (L2) and S6-S7 loops of the other dimer subunit (Fig. 4*B*). The interface is stabilized by both hydrogen bonds and Van der Waals interactions. Main chain hydrogen bonds are formed between residues 168 and 169 of the S4-H1 loop with residues 180 and 178 of the H1-S5 loop of the opposing subunit, respectively, and between residue 207 of the S6-S7 loop with residue 182 of the H1-S5 loop. Side chain hydrogen bonds are also formed in the dimer, and Arg-178 of the H1-S5 loop plays a particularly important role in this regard. The side chain of Arg-178 makes a direct hydrogen bond to the backbone OH of residue 172 of the S4-H1 loop of the opposing subunit and also makes water-mediated interactions to the side chains of Glu-168 and Tyr-160 of the same loop. Van der Waals interactions at the dimer interface involve interactions between Phe-209 of the S6-S7 loop with Ala-182 and Pro-188 of the H1-S5 loop and between Val-169 of the S4-H1 loop with the aliphatic regions of Arg-178 and Ser-180 of the H1-S5 loop.

The dimer interaction in the crystals position the protein segments involved in DNA interaction, the H2 helix and the L1 loop, in a configuration that is incompatible with the simultaneous binding to duplex DNA by both protomers of the dimer. Therefore the dimer in the crystals represents a configuration that is inactive for DNA binding in which each core domain binds a pentameric DNA sequence. The observation that the noncrystallographic trimer mediates identical dimer contacts indicates that the crystallographically observed dimer interface represents a stable minimum. Interestingly, very similar dimer contacts are observed in crystals of the human p53 core domain in the presence of DNA. In these crystals, an asymmetric unit cell contains three p53 core domains and one DNA duplex. Although one p53 protomer is bound specifically to a

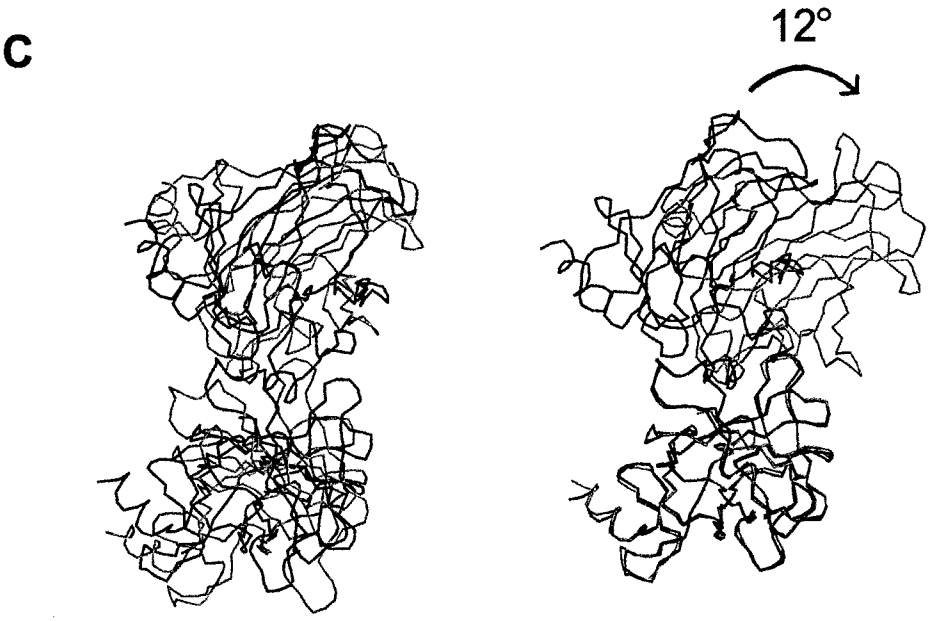

FIG. 4—*continued*

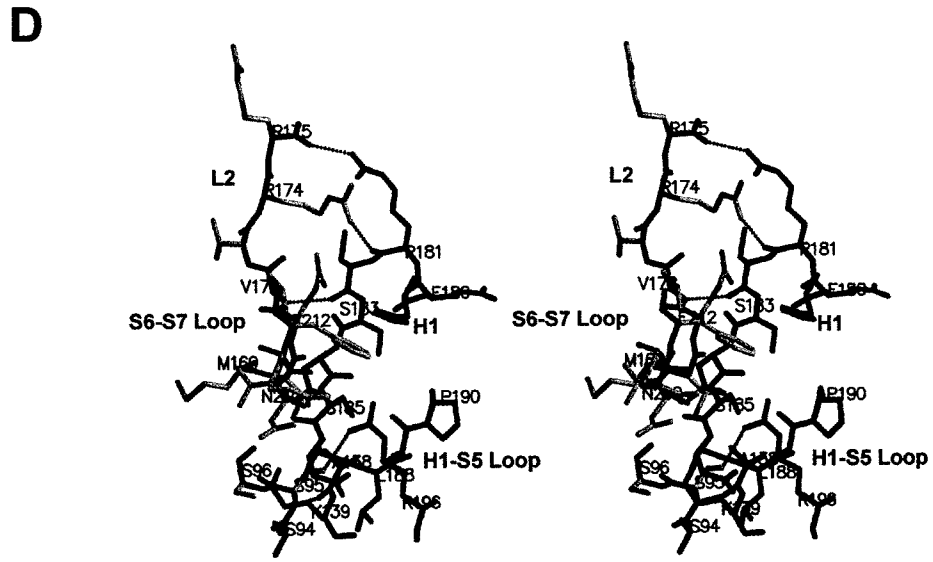

consensus pentameric DNA site, a second p53 protomer is bound nonspecifically at the junction of two DNA duplexes, and a third p53 protomer is not associated with DNA but is involved in dimer contacts with the DNA-binding p53 protomer in the asymmetric unit cell. Strikingly, these dimer contacts are very similar to the dimer contacts that are observed in the DNA-free mouse p53 core domain crystals reported here. Specifically, the same secondary structural elements are involved, the H1-S5 loop of one subunit and the S4-H1 (L2) and S6-S7 loops of the other subunit. Moreover, although the details of the contacts are different, many of the same residues are used to stabilize the dimer. Notably, Arg-174, Arg-181, and Glu-180 (analogous to Arg-171, Arg-178, and Glu-177 in the DNA-free dimer) play important roles in mediating H bonds within the dimer. Phe-212 and Pro-191 (analogous to Phe-209 and Pro-188 in the DNA-free dimer) also mediate Van der Waals interactions within the dimer (Fig. 4*D*).

In addition to the common interactions within the dimer interface of the DNA-free and DNA-containing p53 core domain crystals, there are several divergent interactions resulting in a somewhat different disposition of the two subunits of the dimer when the DNA-bound and DNA-free forms are compared. The overall root mean square deviation between the two p53 dimers is 5.5 Å (Fig. 4*C*). However, a superposition of one of the two subunits reveals that the other subunits of the corresponding dimers are related by a 12 ° rotation of one relative to the other. Taken together, the dimer contacts observed in two different p53 crystal lattices show striking similarity, although there appears to be some flexibility in the details of the interactions that stabilize the dimer.

Biological Implications of Dimer Contacts within the p53 Core Domain—In light of the similar p53 dimer contacts that are present within the crystal lattices of the mouse and human p53 core domain, we investigated the aggregation properties of the mouse p53 core domain in solution. To do this we carried out sedimentation equilibrium ultracentrifugation using two different protein concentrations and three different centrifugation speeds. Analysis of the data revealed a sedimentation profile that could be best fit by a monomer-dimer model fixing the molecular mass to the size of 22,695 Da with a K_d of 2.1 mM

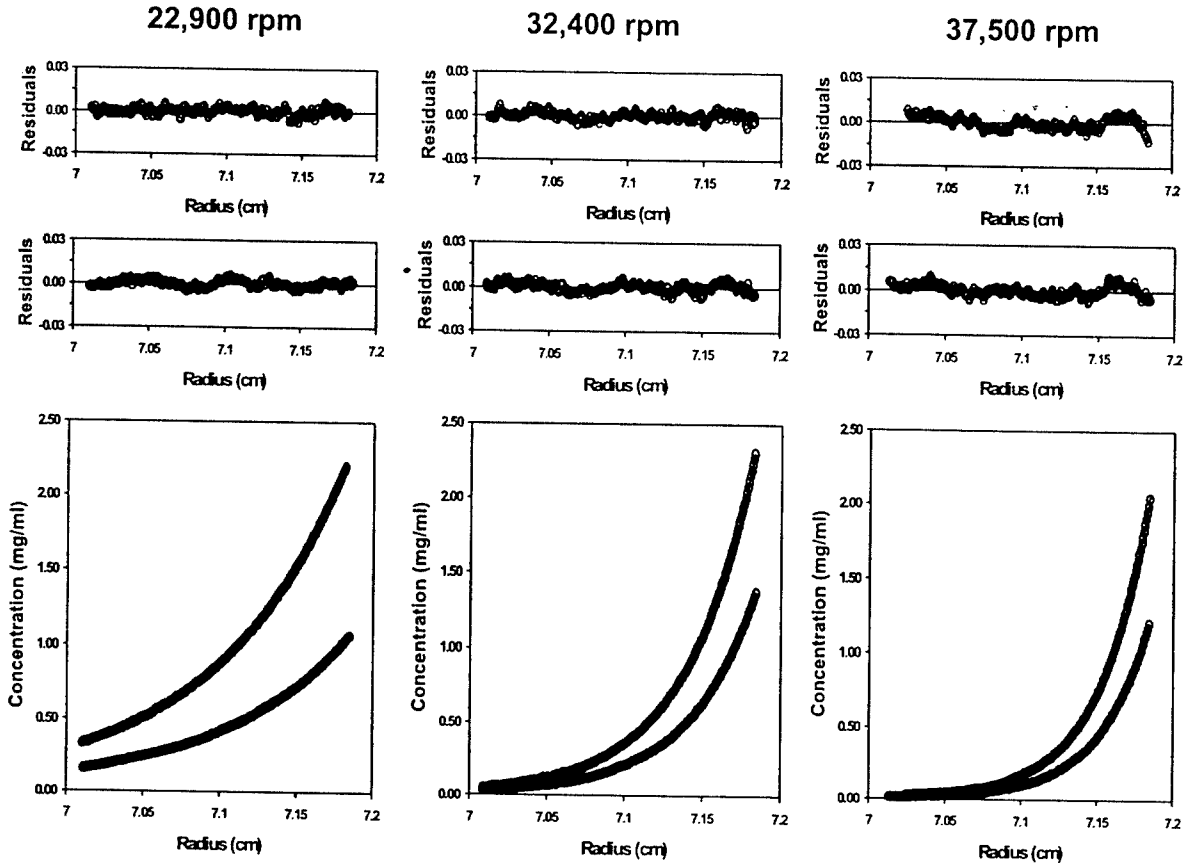

FIG. 5. **Equilibrium sedimentation ultracentrifugation of the mouse p53 core domain.** Two different initial protein concentrations (0.5 mg/ml (*lower curve*) and 1.5 mg/ml (*upper curve*)) were run at each of three different centrifugation speeds (as indicated in the *headings*). The *bottom panels* show concentration distribution plots along the filtered *curves* assuming a single species.

for low levels of dimer formation (Fig. 5). This model for slight oligerimerization, characterizing reversible monomer-dimer equilibrium, was significantly better than a single species model or models describing monomer-trimer or monomer-dimer-tetramer equilibrium. Taken together, the sedimentation equilibrium ultracentrifugation results clearly demonstrate that the isolated mouse p53 core domain is predominantly monomeric at physiological protein concentrations.

In light of these results, what can be the biological implications of the p53 dimer contacts that are observed in the crystals? *In vivo* p53 exists in a tetrameric form largely due to the presence of a highly conserved C-terminal tetramerization domain. Therefore the four *in vivo* p53 core domains are at high local concentrations and furthermore have an enhanced propensity to form specific interactions with each other. Given the tetrameric form of the p53 protein, the most likely interactions between the core domains would be either a dimer of dimers (as observed for the isolated tetramerization domain) or a symmetrical tetramer. For sequence-specific DNA binding, p53 has also been proposed to undergo a conformational change from a state with low affinity for DNA (T state) to a state with high affinity for DNA (R state) (6, 13). These different physiological states of p53 have been proposed based on the activities of antibodies that specifically react with and enhance one of the two states. Based on p53 DNA target sites that are two head to tail decamer repeats of 2-fold symmetric pentameric sites, the p53 conformation with high affinity for DNA is proposed to have the core domains aligned as two 2-fold symmetric dimers. Based on our crystallographic results, we propose that in the context of the p53 tetramer the core domain is arranged as a dimer of dimers and that the core domain dimer observed in our crystals represents a low affinity DNA state. This is consistent with the observation that the dimer in our crystals is

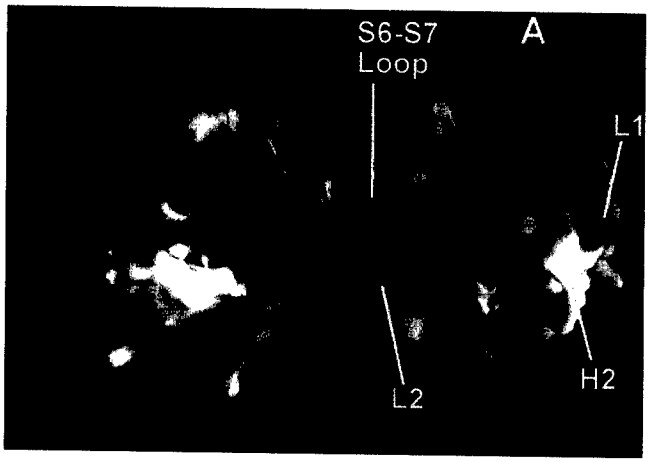

FIG. 6. **Electrostatic surface of the mouse p53 core domain dimer.** The electrostatic potential is calculated with the program GRASP (Nicholls *et al.*, 1991) and displayed as a color gradient from *red* (electronegative ≤ -10 kilotesla/charge) to *blue* (electropositive, ≥ 10 kilotesla/charge). *A* and *B* indicate subunits A and B of a noncrystallographic dimer of the unit cell.

configured in such a way that it is incompatible with simultaneous binding to duplex DNA. It is also consistent with the observation that a similar dimer is observed in the crystals of the human p53 core domain in the presence of DNA and in which only one of two subunits of the dimer make specific contacts to DNA. An electrostatic potential energy surface of the p53 core domain dimer in our crystals revealed a pronounced electropositive charge patch along one face of the dimer (Fig. 6). This surface may form a docking site for an acidic region of the p53 protein such as the N-terminal transactivation domain in the low affinity DNA binding state. Such

an interaction would also serve to mask the transactivation domain of p53 prior to high affinity DNA binding.

In conclusion, we have determined the crystal structure of the mouse p53 core domain and have compared it with the DNA-bound form of its human homologue. The comparison reveals that DNA binding by the core domain is accompanied by the reconfiguration of a loop region for major groove interactions with the DNA. Strikingly, we observe dimers of p53 core domains in our crystals in a configuration that is incompatible with simultaneous binding of both subunits to duplex DNA. A comparison with a similarly configured dimer in crystals of the human p53 core domain suggests that this dimer may represent a physiologically relevant low affinity DNA binding state of the p53 core domains in the context of the intact p53 tetramer. Further insights into the structural rearrangements mediated by p53 as a function of DNA binding will require structural analysis of the intact p53 tetramer in the presence and absence of DNA.

Acknowledgment—We thank Irina Kriksunov and Marian Szebenyi for help on beamline A1 at Cornell High Energy Synchrotron Source and R. Burnett for useful discussions.

REFERENCES

1. Prives, C., and Hall, P. (1999) *J. Pathol.* **187,** 112–126
2. Burns, T. F., and El-Deiry, W. S. (1999) *J. Cell. Physiol.* **181,** 231–239
3. Levine, A. J. (1997) *Cell* **88,** 323–331
4. Cho, Y., Gorina, S., Jeffrey, P. D., and Pavletich, N. P. (1994) *Science* **265,** 346–355
5. El-Deiry, W. S., Tokino, T., Velculescu, V. E., Levy, D. B., Parsons, R., Trent, J. M., Lin, D., Mercer, W. E., Kinzler, K. W., and Vogelstein, B. (1993) *Cell* **75,** 817–825
6. Halazonetis, T. D., and Kandil, A. N. (1993) *EMBO J.* **12,** 5057–5064
7. Friedman, P. N., Chen, X. B., Bargonetti, J., and Prives, C. (1993) *Proc. Natl. Acad. Sci. U. S. A.* **90,** 3319–3323
8. Stenger, J. E., Tegtmeyer, P., Mayr, G. A., Reed, M., Wang, Y., Wang, P., Hough, P. V. C., and Mastrangelo, I. A. (1994) *EMBO J.* **13,** 6011–6020
9. Pavletich, N. P., Chambers, K. A., and Pabo, C. O. (1993) *Genes Dev.* **7,** 2556–2564
10. Wang, Y., Reed, M., Wang, P., Stenger, J. E., Mayr, G., Anderson, M. E., Swhwedes, J. F., and Tegtmeyer, P. (1993) *Genes Dev.* **7,** 2575–2586
11. Tokino, T., Thiagalingam, S., Eldeiry, W. S., Waldman, T., Kinzler, K. W., and Vogelstein, B. (1994) *Hum. Mol. Genet.* **3,** 1537–1542
12. El-Deiry, W. S., Kern, S. E., Pietenpol, J. A., Kinzler, K. W., and Vogelstein, B. (1992) *Nat. Genet.* **1,** 45–49
13. Waterman, J. L. F., Shenk, J. L., and Halazonetis, T. D. (1995) *EMBO J.* **14,** 512–519
14. Clore, G. M., Ernst, J., Clubb, R., Omichinski, J. G., Kennedy, W. M., Sakaguchi, K., Appella, E., and Gronenborn, A. M. (1995) *Nat. Struct. Biol.* **2,** 253–254
15. Jeffrey, P. D., Gorina, S., and Pavletich, N. P. (1995) *Science* **267,** 1498–1502
16. Lee, W., Harvey, T. S., Yin, Y., Litchfield, D., and Arrowsmith, C. H. (1994) *Nat. Struct. Biol.* **1,** 877–890
17. Leslie, A. G. W. (1992) in *CCP4 and ESF-EACMB Newsletter on Protein Crystallography*, Darsbury Laboratory, Darsbury, U. K.
18. Navaza, J. (1994) *Acta Crystallogr. Sect. A* **50,** 157–163
19. Jones, T. A. (1978) *J. Appl. Crystallogr.* **11,** 268–272
20. Brunger, A. T., Adams, P. D., Clore, G. M., DeLano, W. L., Gros, P., Grosse-Kunstleve, R. W., Jiang, J. S., Kuszewski, J., Nilges, M., Pannu, N. S., Read, R. J., Rice, L. M., Simonson, T., and Warren, G. L. (1998) *Acta Crystallogr. Sect. D Biol. Crystallogr.* **54,** 905–921
21. Brunger, A. T., and Krukowski, A. (1990) *Acta Crystallogr. Sect. A* **46,** 585–593
22. Rice, L. M., and Brunger, A. T. (1994) *Proteins* **19,** 277–290
23. Jiang, J. S., and Brunger, A. T. (1994) *J. Mol. Biol.* **243,** 100–115
24. Yphantis, D. A. (1964) *Biochemistry* **3,** 297–317
25. Johnson, M. L., Correia, J. J., Yphantis, D. A., and Halvorson, H. R. (1981) *Biophys. J.* **36,** 575–588
26. Laue, T. M., Shah, B. D., Ridgeway, T. M., and Pelletier, S. L. (1992) in *Analytical Ultracentrifugation in Biochemistry and Polymer Science* (Harding, S. E., Rowe, A. J., and Horton, J. C., eds) pp. 90–125, The Royal Society of Chemistry, Cambridge, U. K.
27. Nicholls, A., Sharp, R. A., and Honig, B. (1991) *Proteins* **11,** 281–296